

#### **PAPER**

Manufacturing of stereolithographic 3D printed boron nitride nanotube-reinforced ceramic composites with improved thermal and mechanical performance

To cite this article: Mehul Tank et al 2023 Funct. Compos. Struct. 5 015001

View the article online for updates and enhancements.

## You may also like

- Towards sustainable transparent flexible heaters: Integration of a BNNT interlayer using green solvent substitution Kaitlin Wagner, Shan Zou, Yadienka Martinez-Rubi et al.
- <u>Boron nitride nanotube scaffolds:</u>
  <u>emergence of a new era in regenerative</u>
  <u>medicine</u>
  Sathyan Vivekanand Anandhan and Uma
  Maheswari Krishnan
- Density functional theory study of Cudoped BNNT as highly sensitive and selective gas sensor for carbon monoxide Guohong Fan, Xiaohua Wang, Xianxian Tu et al.

# **Functional Composites and Structures**



#### RECEIVED

28 September 2022

#### REVISED

2 December 2022

## ACCEPTED FOR PUBLICATION 5 January 2023

PURIISHED

25 January 2023

#### **PAPER**

# Manufacturing of stereolithographic 3D printed boron nitride nanotube-reinforced ceramic composites with improved thermal and mechanical performance

Mehul Tank<sup>1,2</sup>, Ana De Leon<sup>1,2</sup>, Wentao Huang<sup>3</sup>, Mitesh Patadia<sup>1,2</sup>, Joshua Degraff<sup>1,2</sup> and Rebekah Sweat<sup>1,2,\*</sup>

- FAMU-FSU College of Engineering, 2525, Pottsdamer Rd, Tallahassee, FL, United States of America
- <sup>2</sup> High-Performance Materials Institute (HPMI), 2005, Levy Avenue, Tallahassee, FL, United States of America
- Department of Engineering Science, Trinity University, One Trinity Way, San Antonio, TX, United States of America
- \* Author to whom any correspondence should be addressed.

E-mail: r.sweat@eng.famu.fsu.edu

**Keywords:** boron nitride nanotubes, multifunctional nanotubes, stereolithographic 3D printing, printed ceramic, fused silica, high-temperature processing, nanotube modeling

Supplementary material for this article is available online

#### **Abstract**

Boron nitride nanotubes (BNNTs) are the perfect candidate for nanofillers in high-temperature multifunctional ceramics due to their high thermal stability, oxidation resistance, good mechanical properties, high thermal conductivity, and radiation shielding. In this paper, 3D printed ceramic nanocomposite with 0.1 wt% of BNNT was prepared by fusing it at high temperatures. Samples were built with three different print directions to study the effect of print layers on mechanical performance along with BNNT addition. Dynamic mechanical analysis is performed to study the length effect of nanoscale reinforcements on the mechanical properties of the printed ceramic composites reporting significant improvements up to 55% in bending strength and 72% in bending modulus with just 0.1 wt% BNNT addition. A 63% thermal diffusivity improvement of ceramic by adding BNNTs is observed using laser flash analysis. The bridging and pull-out effect of nanotubes with a longer aspect ratio was observed with high-resolution microscopy. Such composites' modeling and simulation approaches are crucial for virtual testing and industrial applications. Understanding the effect of nanoscale synthetic fillers for 3D printed high-temperature ceramics can revolutionize future extreme environment structures.

#### 1. Introduction

Additive manufacturing (AM), or three-dimensional (3D) printing, is a fast-developing technology that enables physical items to be graphically created on a computer and generated using a layer-by-layer model. As a result, the freedom and simplicity of customization in digital design make it possible to direct fabricate functional structures with complex shapes, which are frequently required in the aerospace, biomedical, and electronic sectors [1–4].

With increased interest, AM has become more accessible and affordable. Fused deposition molding, stereolithography (SLA), and selective laser sintering (SLS) are some of the AM processes available. SLA 3D printing is a process that uses photosensitive polymer (PSP) resins as the starting material. SLA printing enhances printing resolution up to 100 times compared to other 3D printing technologies that employ solid polymer filament as the starting material [3]. A broad range of ceramic SLA and related AM methods involving photopolymerization of ceramic powder suspensions has been studied in the past [5–7].

It is well known that incorporating nanoscale reinforcements such as nanotubes into the ceramic matrix improves the mechanical properties of a composite [8]. For a high-temperature application, boron nitride nanotubes (BNNTs) are one of the perfect nanofiller candidates that can be used to enhance mechanical and thermal conductivity performance in ceramic matrix nanocomposites. Following the discovery of carbon

nanotubes (CNTs) in the early 1990s, tubular structures of boron nitride were theorized in 1994 [9, 10]. The BN structure is similar to the hexagonal lattice structure seen in sp³-hybridized carbon–carbon bonds of graphene and CNTs. The first successful synthesis and observation of BNNTs occurred in 1995, becoming the first inorganic nanotube [11]. Due to their structure, BNNTs possess excellent mechanical properties similar to CNTs. With a tensile strength of 33 GPa [12], Young's modulus of 1.3 TPa [13, 14], a bending modulus of 760 GPa [15], and a shear modulus of 7 GPa [15], they are an obvious candidate for fiber-reinforced composite materials. In addition to their excellent mechanical properties, BNNTs are more thermally stable in oxidative environments than CNTs. Many studies have shown that BNNTs remain stable up to 850 °C in air [16, 17]. The thermal stability of BNNTs has also been studied through Joule heating under vacuum [18]. It was estimated that the dissociation of the B–N bond and failure of nanotubes occurred at temperatures up to 1900 °C depending on tube geometry. A recent study reported that B–N structures of BNNTs are completely stable up to 1800 °C in inert environments, introducing confident use of high-temperature manufacturing processing on BNNT composites [19].

BNNTs have a high thermal conductivity of  $\sim$ 350 W m<sup>-1</sup> K<sup>-1</sup>, comparable to CNTs and many metals [20]. In addition to that, with outstanding mechanical and thermal properties, BNNTs are electrical insulators with a wide bandgap of B–N bonds of 5–6 eV [21, 22], while CNTs are metallic or semiconductors [23]. Due to the low atomic number of elements, BNNTs have been among the most effective materials for neutron capture. BNNT's geometric features, including high surface area and aspect ratios, offer both mechanical support and radiation shielding capability, which makes it suitable for structural materials of space crafts or astronaut suits [24–26].

Due to their robust and lightweight tubular nanostructure, BNNTs hold enormous potential as a reinforcing additive in ceramics. In the past literature, significant mechanical property improvements in BNNT reinforced ceramic matrix nanocomposite have been documented. A hot press fabricated BNNT/G18 glass composite with 4 wt% BNNT was noted to improve its flexural strength and fracture toughness by 90% and 35%, respectively [27]. Similarly, introducing just 1 wt% BNNT to alumina ( $Al_2O_3$ ) and zirconia ceramic increased toughness by 35% and 65%, respectively [28, 29]. The addition of 5% BNNT to silica ( $SiO_2$ ) increases fracture strength and toughness by 131% and 109%, respectively, due to microstructural changes [30]. With 1.5 vol% of BNNTs, spark plasma sintered BNNT/ $\alpha$ -Al $_2O_3$  composite was observed to reduce grain size by 50%, and microhardness increased by 22% [31]. A recent comparative study comparing the interfacial strength properties of BNNT/silica and CNT/silica ceramic matrix composite measured  $\sim$ 55% higher interfacial shear strength for BNNT/silica than for CNT/silica [32, 33]. Along with mechanical enhancements, BNNTs create a high-temperature thermally conductive network and increase thermal conductivity with preserved electrical insulating properties of ceramic matrices [34]. Therefore, BNNTs are perfect candidates for nano reinforcement fillers for ceramic matrix composites.

This unique combination of thermal conduction, electrical insulation properties, and radiation shielding properties opens a wide range of space instrument applications, such as space rovers. A distinctive approach is to use BNNTs as nanofillers for improved thermal diffusivity and mechanical properties of 3D-printed fused ceramic composites for high-temperature applications. Therefore, the fast-developing and high precession stereolithographic (SLA) 3D printing technique is adopted to characterize ceramic nanocomposites with BNNTs as fillers. As BNNTs have a high aspect ratio at the nanoscale, the geometry effects of synthetic fillers towards reinforcement are studied for 3D-printed fused ceramics for high-temperature space applications. Furthermore, their contribution to the ceramic matrix is also studied with the modeling and simulation approach, which further helps expedite the development of new materials.

#### 2. Experimental

#### 2.1. Materials, mixing, and printing

Ceramic resin consisting of PSP and infused silica particles from Formlabs (Somerville, MA) was used for 3D printing. Nanocomposite ceramic resin was made by dispersing purified multi-walled BNNTs in dimethylformamide (DMF). Purified multi-walled BNNTs puffballs with 2–5 walls were provided by BNNT materials. The ratio of BNNT content in ceramic resin (after fusing) was set at 0.1%. The silica content in the polymer/silica resin was found through thermogravimetric analysis (TGA) on the neat sample. TGA was carried out using a Q50 TGA (TA Instruments, New Castle, DE, USA) in air with a temperature ramp rate of 20 °C min<sup>-1</sup> from 25 °C to 750 °C with a 20 min isothermal hold at 750 °C. About 30–35 mg of neat ceramic sample was used to measure actual silica content. While heating in TGA, the binder polymer completely burned out over 500 °C, leaving 70.94% silica by weight at the end, as seen in figure 1. The weight of nanofillers to be added into resin for printing ceramic nanocomposites are chosen so that the mixture contains 0.1 wt% of nanofillers of the silica content in the resin.

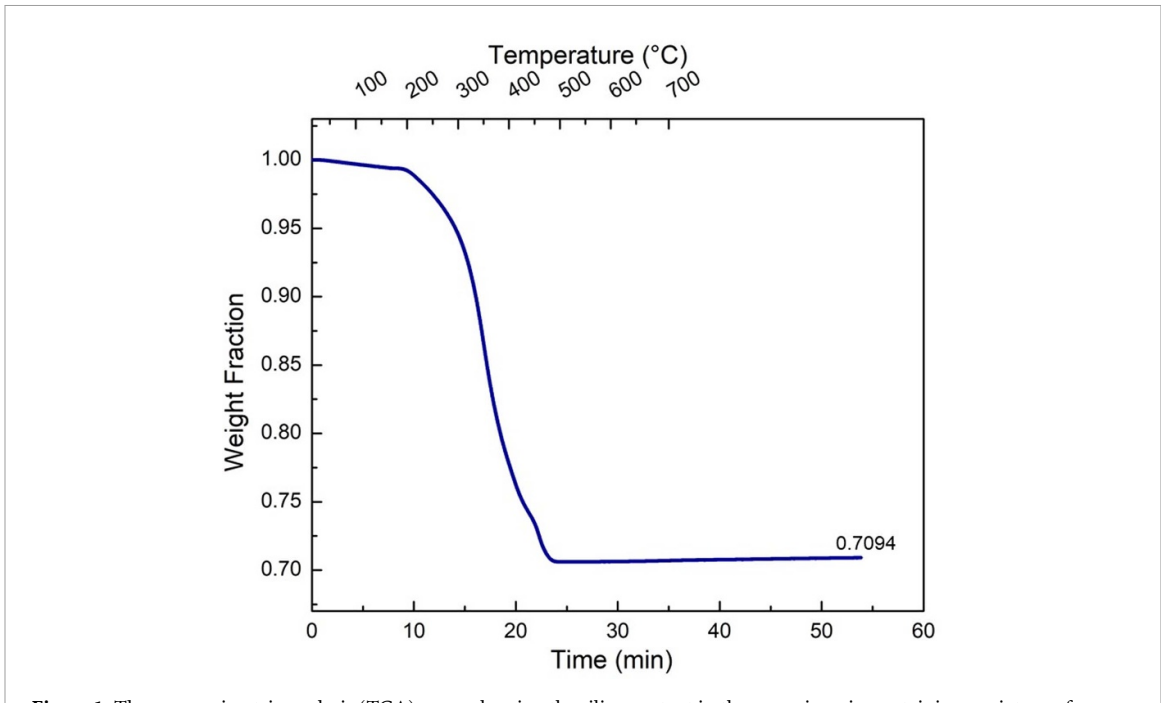


**Figure 1.** Thermogravimetric analysis (TGA) curve showing the silica content in the ceramic resin containing a mixture of photosensitive polymer and silica.

The BNNT puffballs were broken into smaller fragments in DMF and set on a magnetic stirrer (ThermoFisher Scientific, Waltham, MA) at room temperature for 96 h with the spin speed set to 120 rpm, followed by 30 min of bath sonication in a Cole-Parmer Ultrasonic Cleaner (Vernon Hills, IL). Similar to a previous study on BNNT dispersion by Tiano *et al* [35], a well-dispersed swollen DMF/BNNT solution was achieved at the end of bath sonication. Photosensitive Ceramic Resin was slowly added, and the DMF/BNNT/ Resin solution was stirred continuously at 200 rpm for 120 h at 80 °C on a ThermoFisher hot plate to evaporate DMF from the mixture using an Arrow 1750 Laboratory Mixer (Hillside, NJ) to avoid any settling or cluster formation in the mixture. The complete evaporation of DMF from the DMF/BNNT/Resin at the end of 120 h was ensured by comparing the weight and volume of the solution before and after the evaporation. Figure 2 shows the schematic layout of the manufacturing process toward characterization steps.

The neat and BNNT nanocomposite samples were printed using a Form 2 desktop SLA 3D printer by Formlabs (Somerville, MA). The samples were printed with three different growth directions (type A- growth along the length, type B- growth along the width, and type C- growth along the thickness) as shown in figure 3 on the print platform with 100  $\mu$ m layers. The printed green-state parts were washed in a Formlabs Form Wash (Sommerville, MA) with isopropanol for 10 min to remove any uncured resin around the samples and polished slightly to fit the dimensional specifications if needed.

#### 2.2. Polymer burnout and ceramic fusing

While sintering the silica particles, the stability of the fillers must be confirmed at high temperatures to prevent nanofillers from being damaged. Previously, studies have reported that the BNNTs have high oxidation resistance of  $\sim$ 850 °C [16, 17], and a recent study confirms the complete stability of the BNNTs up to 1800 °C in inert environments [19]. In order to prevent oxidation of BNNTs above 850 °C in air during the sintering process, the sintering process was divided into two steps (1) polymer burnout stage in the air up to 750 °C (figure 4(a)) and (2) fusing stage in an inert environment up to 1275 °C (figure 4(b)).

The green state samples first underwent a polymer burnout cycle where samples were heated at a 2 °C ramp rate up to 750 °C with a hold of 2 h at 240 °C and 1 h at 300 °C in a Lindberg/Blue M box furnace (ThermoFisher Scientific, Waltham, MA) in air to burn out binder polymer from the printed samples. To avoid oxidation of the BNNT in air, the samples were held for 20 min at 750 °C to further ensure complete evaporation of the binder polymer from the ceramic samples. After polymer burnout, the ceramic powder samples containing BNNT and loose silica particles were transferred to a GSL-1700X tube furnace (MTI Corporation, Richmond, CA) for fusing in a nitrogen atmosphere, where the samples were heated at a ramp rate of 5 °C min<sup>-1</sup> to 1275 °C. With a hold of 20 min at 1275 °C, samples were cool down at a controlled rate of 5 °C min<sup>-1</sup> up to 800 °C and at a free fall with the furnace up to room temperature. The samples

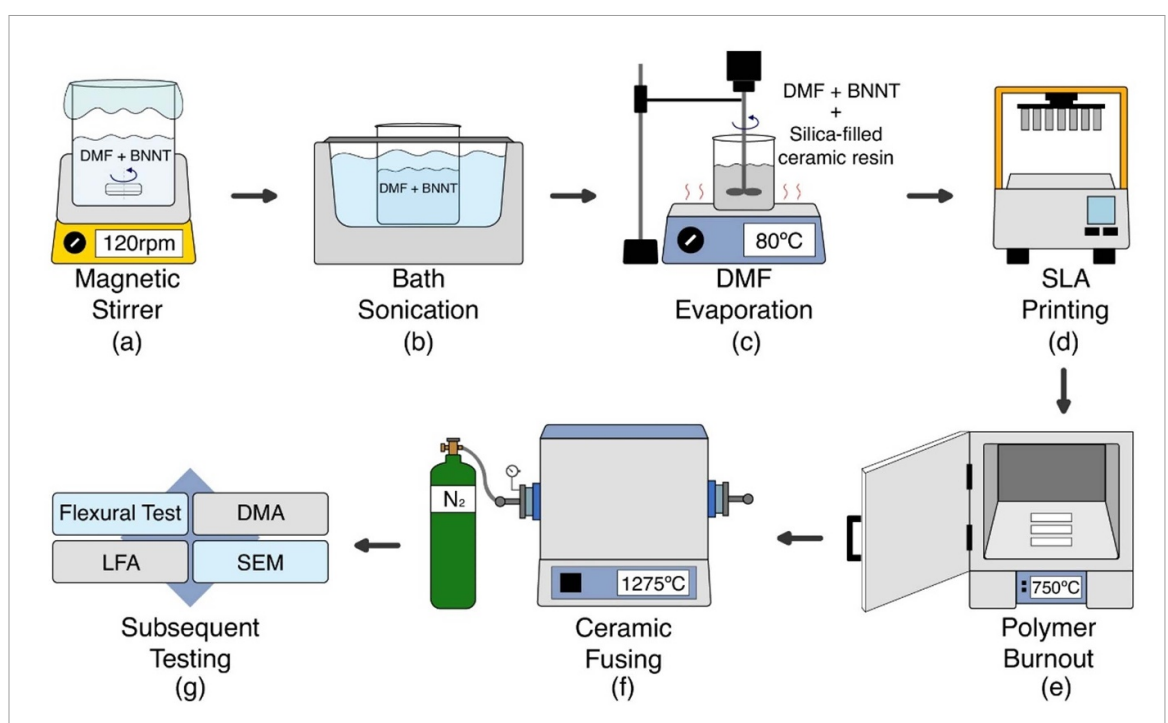


**Figure 2.** Schematic layout of the manufacturing process of BNNT/silica nanocomposites. Figures (a)–(c) shows the manufacturing process of BNNT nanocomposite resin, which includes BNNT dispersion through a magnetic stirrer followed by bath sonication and evaporation of dispersion solvent. (d) Printing of test samples through SLA printing. Figures (e), (f) ceramic sintering involves polymer burnout and the ceramic fusing stage. (g) Subsequent testing was performed in this study.

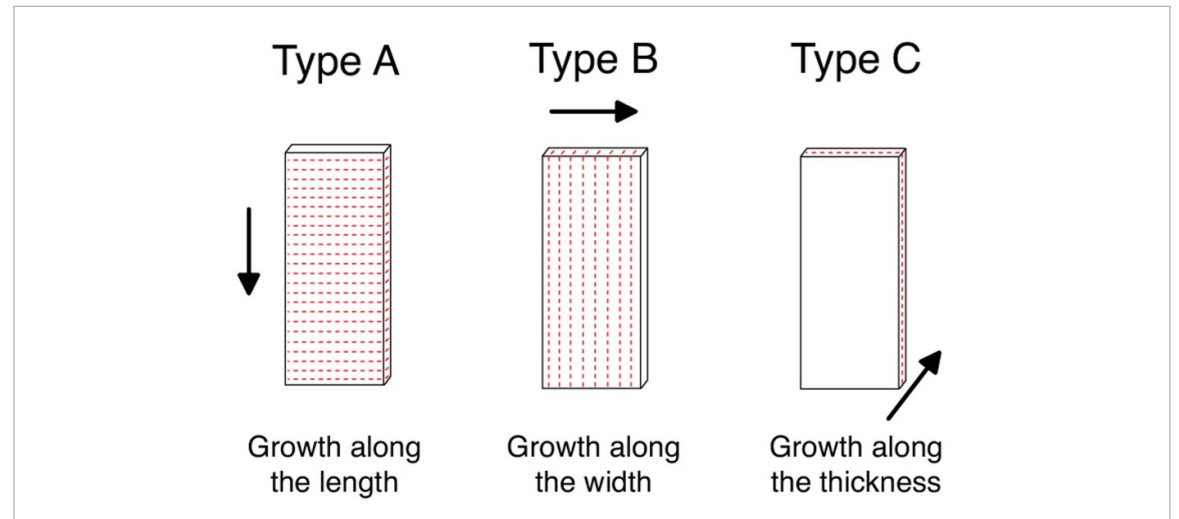
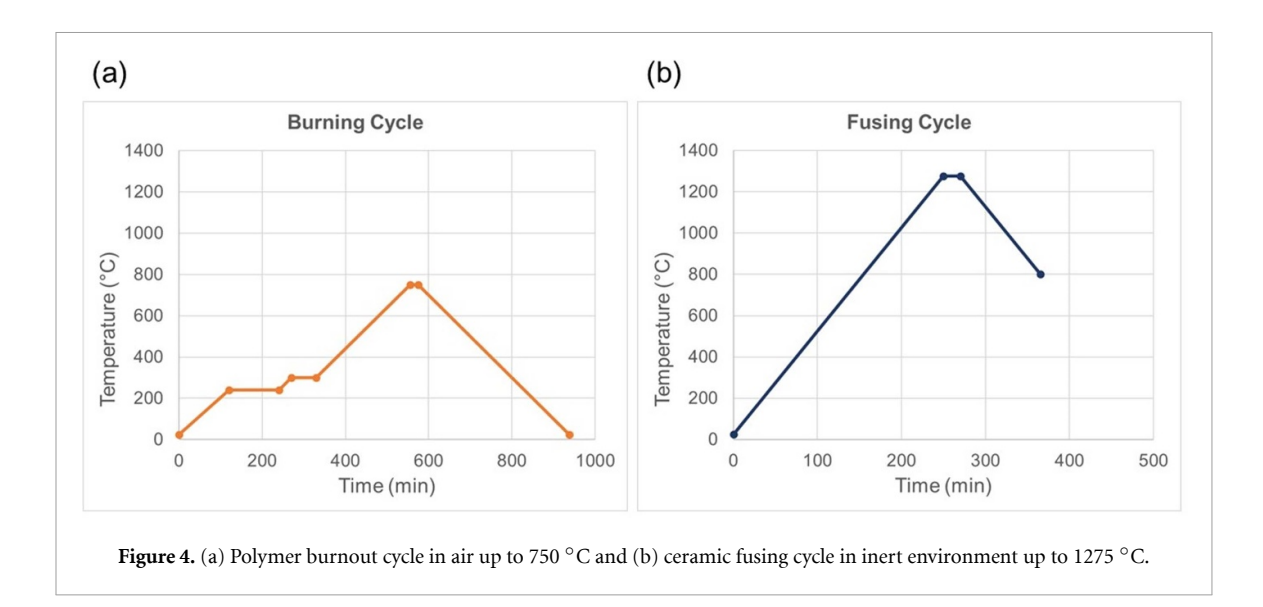


**Figure 3.** Samples printed in three different print directions (a) type A samples with growth along the length, (b) type B samples with growth along the width, and (c) type C samples with growth along the thickness.

were removed from the furnace at room temperature for test and analysis. Neat samples were prepared using the same method applied to nanocomposites to ensure an accurate comparison. Figure 5 shows the pictures of samples after printing (figure 5(a)), burnout stage (figure 5(b)), and fusing stage (figure 5(c)) taken during the experiment. The SEM inset demonstrates surface consistency, with some pores visible due to the consolidation processes.

#### 2.3. Dynamic mechanical analysis (DMA) and mechanical testing

DMA was performed using an ARES-G2 (TA Instruments, New Castle, DE, USA) in a three-point bend mode to evaluate the mechanical properties of the composite materials. A three-point bend setup based on ASTM C1161-18 with a 25 mm support span and frequencies from 1 Hz to 10 Hz with a max strain of 0.05% is used to evaluate the bending modulus. A crosshead speed of 2 mm min<sup>-1</sup> is used to determine the bending strength of fused samples with a width of  $\sim$ 10 mm and thickness of  $\sim$ 2 mm at room temperature, as shown in figure 6. Five replications of each type of sample were performed for both dynamic mechanical frequency



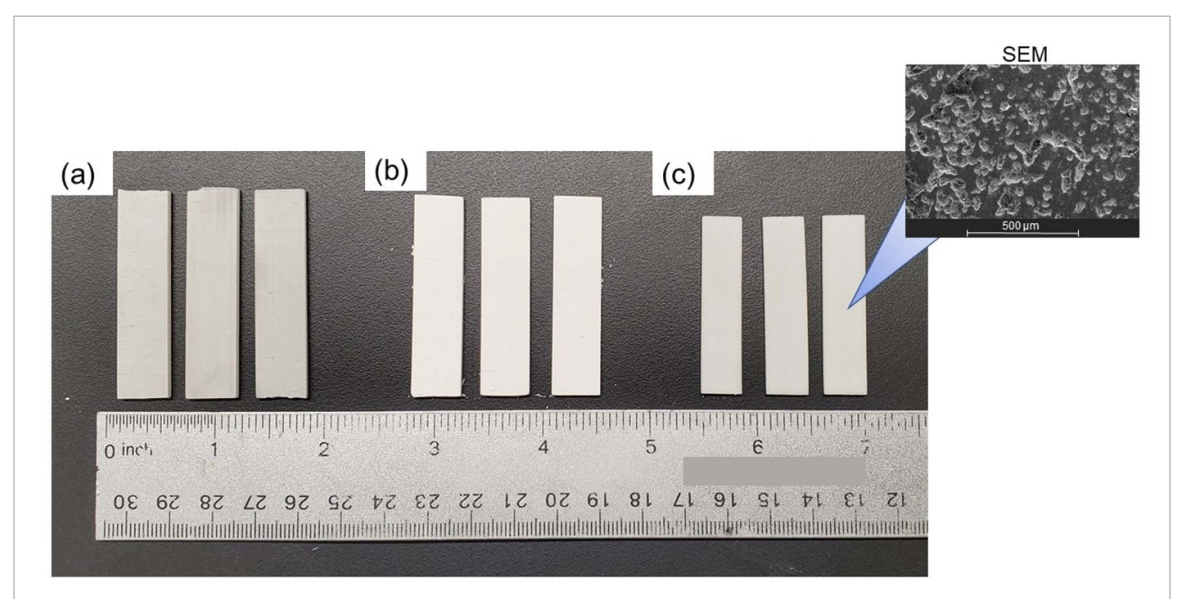


**Figure 5.** Photo of (a) printed samples, (b) samples after the polymer burnout cycle (c) fused samples ready to test after the fusing cycle. The inset shows the SEM image of fused ceramics.

sweep analysis and a fracture test to confirm the repeatability of the results. The results were further analyzed through statistical analysis for a better comparison of results between neat and nanocomposites. Material toughness for brittle ceramics was calculated through the area under the stress–strain curve up to the peak stress value for better comparability.

#### 2.4. Statistical analysis

Statistical design, performed in Minitab Statistical Software, categorizes the mechanical performance of 3D-printed fused ceramic composites. Figure 7 shows the two-way analysis of variance (ANOVA) design applied in this study to determine how two independent factors at different levels affect a response. The factors of interest in this study are BNNT addition with two levels (0.1 wt% BNNT and Neat) and printing type with three levels (type A, type B, and type C). Separate analyses were performed to observe the significance of each factor on the study's responses (modulus and strength). Confidence intervals through Fisher's least significant difference (LSD) method were created for all pairwise differences between factor level means.

#### 2.5. Scanning electron microscopy (SEM)

SEM imaging was conducted using a Helios G4 UC (Thermo Fisher Scientific, Waltham, MA, USA) operating at 5 kV accelerating voltage with an ETD detector. A gold sputter coating of 5 nm was applied. The magnification and scale bars are shown at the bottom of each image.

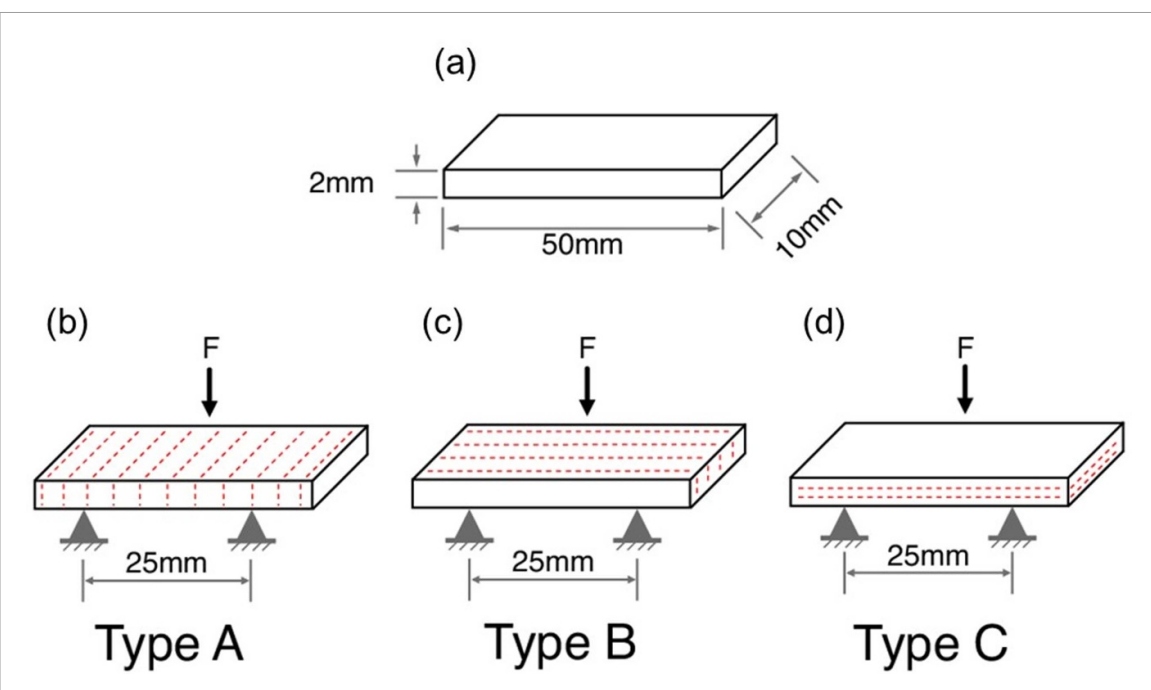


**Figure 6.** (a) Average sample dimensions after fusing. (b)–(d) The three types of samples (type A, type B, and type C) under a typical three-point bend setup with a 25 mm support span.

2 x 3 Two-Way ANOVA for 3D printed BNNT Ceramic Nanocomposites				
2 factors: BNNT Addition * Printing Type				
Responses:- • Strength • Modulus		Printing Type		
		Type A	Туре В	Type C
BNNT Addition	0.1 wt% BNNT	BNNT A	BNNT B	BNNT C
	Neat	Neat A	Neat B	Neat C

Figure 7. Statistical design,  $2 \times 3$  two-way ANOVA, applied in this study for the mechanical characterization of 3D-printed BNNT ceramic nanocomposites.

#### 2.6. Thermal diffusivity testing

Using the standard apparatus, the laser flash thermal diffusivity measurements were carried out with the Netzsch LFA 457 on a  $10 \times 10 \times 2$  mm sample. A laser beam is directed to the bottom of the sample, and the temperature rise on the top surface of the sample is then measured using the IR detector. The samples were coated with a graphite spray to eliminate any reflection of laser from the incident surface or transparency of the sample to obtain a good detector signal. The thermal diffusivity measurement on three different samples of type C, with each subject to five measurements, was performed on neat and BNNT/ceramic composites.

#### 2.7. Abbreviations and naming conventions

Neat A: Control samples without BNNT addition printed in the 'A' direction having growth along the length of the sample as mentioned in section 2.1.

Neat B: Control samples without BNNT addition printed in the 'B' direction having growth along the width of the sample as mentioned in section 2.1.

Neat C: Control samples without BNNT addition printed in the 'C' direction having growth along the thickness of the sample as mentioned in section 2.1.

BNNT A: Nanocomposite samples with 0.1 wt% BNNT addition printed in the 'A' direction having growth along the length of the sample as mentioned in section 2.1.

BNNT B: Nanocomposite samples with 0.1 wt% BNNT addition printed in the 'B' direction having growth along the width of the sample as mentioned in section 2.1.

BNNT C: Nanocomposite samples with 0.1 wt% BNNT addition printed in 'C' direction having growth along the thickness of sample as mentioned in section 2.1.

#### 3. Results and discussion

#### 3.1. Two-way analysis of variance (ANOVA)

A two-way ANOVA was performed to determine a statistically significant difference between the means of independent groups on the mechanical performance of 3D printed ceramic nanocomposites to understand the reproducibility, reliability, and comparability of the results. Figures 8(a), (c), and 9(a), (c) shows the interaction plots explaining the combined effect of BNNT addition and printing type on the strength and modulus of the composite, respectively. The individual means of calculated flexure strength and modulus of ceramic composites with their standard deviation (shown through error bars) between replications are shown in figures 8(b) and 9(b), respectively.

The increasing trend in both strength and modulus of neat samples along the print direction (from type A to type C) can be seen in figures 8(a) and 9(a), respectively. The previous study on 3D printed neat silica has reported a similar increasing trend of flexural strength across the print direction from type A to type C, as observed in this study [36]. Literature has reported a flexural strength of neat 3D printed silica in the range of 6–18 MPa with fusing temperatures ranging from 1200 °C to 1300 °C, which perfectly aligns with the current report [36-39]. However, BNNT nanocomposites' strength and modulus increase along the print direction from sample type A to type B and decrease slightly from sample type B to type C. The interaction plots across BNNT addition, figures 8(c) and 9(c) for strength and modulus, respectively, further depict that the print direction B shows a positive interactive effect and gives a substantial improvement of 54.98% and 51.62% in flexure strength and modulus of the ceramics respectively through the addition of BNNTs. By adding BNNTs, printing type A and type C also showed significant improvement and modulus of 43.03% and 15.24% in strength and 72.04% and 10.58% in modulus, respectively. Overall, the neat ceramics showed an average modulus of 8.75 GPa and a strength of 11.84 MPa, while BNNT/ceramic samples showed an average modulus of 11.99 GPa and a strength of 16.11 MPa across all three print directions. Overall, the material toughness of the silica composites was observed to be improved by 17.58% from 10.33 to 12.15 kJ m<sup>-3</sup> with the addition of just 0.1 wt% BNNTs. Figure 10 shows the stress–strain curves of neat and BNNT composite samples. The addition of BNNTs to a porous ceramic shows a positive synergetic effect and improves matrix material modulus extraordinarily. Ceramic matrix materials contain air voids, which can be greatly assisted by well-dispersed high aspect ratio fillers even more than the theoretical rule of mixtures due to factors such as pores and dispersion.

Additionally, considering the individual standard deviation, Fisher's LSD was calculated and used to create intervals for all pairs of means and make direct comparisons between two means from both groups. Figures 8(d) and 9(d) show the LSD intervals of all 15 combinations of strength and modulus, respectively. The intervals of pairs that do not contain zero are considered statistically significant.

By comparing the mean of responses through Fisher's LSD, it can be stated that print direction significantly affects the strength and modulus of the neat and BNNT composite. Only the strength and modulus of neat ceramics between type B and type C are statistically insignificant (marked through the red circle in figures 8(d) and 9(d)). Additionally, BNNT addition across all three print directions has a significant effect on the strength and modulus compared to neat ceramics. In conclusion, two-way ANOVA proved that BNNT addition has a statistically significant improvement on the mechanical performance of 3D printed fused ceramics across all three print directions proving themselves a perfect candidate for future high-performance materials for high-temperature or space instruments applications.

The three-point bending mechanical results are seen in figure 10. All sample types demonstrated a linear stress/strain relationship near the failure point. A significant increase in modulus is evident from print directions *A* to *B* and *C*. The major increase in strength is also noted for the BNNT in print direction *B*, which is the highest performance for modulus and strength. Failure strain is higher in type A samples since the individual layers do not act as continuous beams across the entire span. Type B and type C having individual layers acting as a continuous beam across the entire span of the three-point bend testing system, which explains pure toughening of ceramic through the addition of BNNT with negligible change in failure strain.

#### 3.2. Scanning electron microscopy (SEM)

The fractured surface of specimens tested in three-point bend testing was observed through SEM. Well-dispersed BNNT sites on the fractured surface of BNNT/silica samples were captured during SEM analysis. Marker '1' in figure 11 shows the region having individual nanotubes nicely embedded in the silica

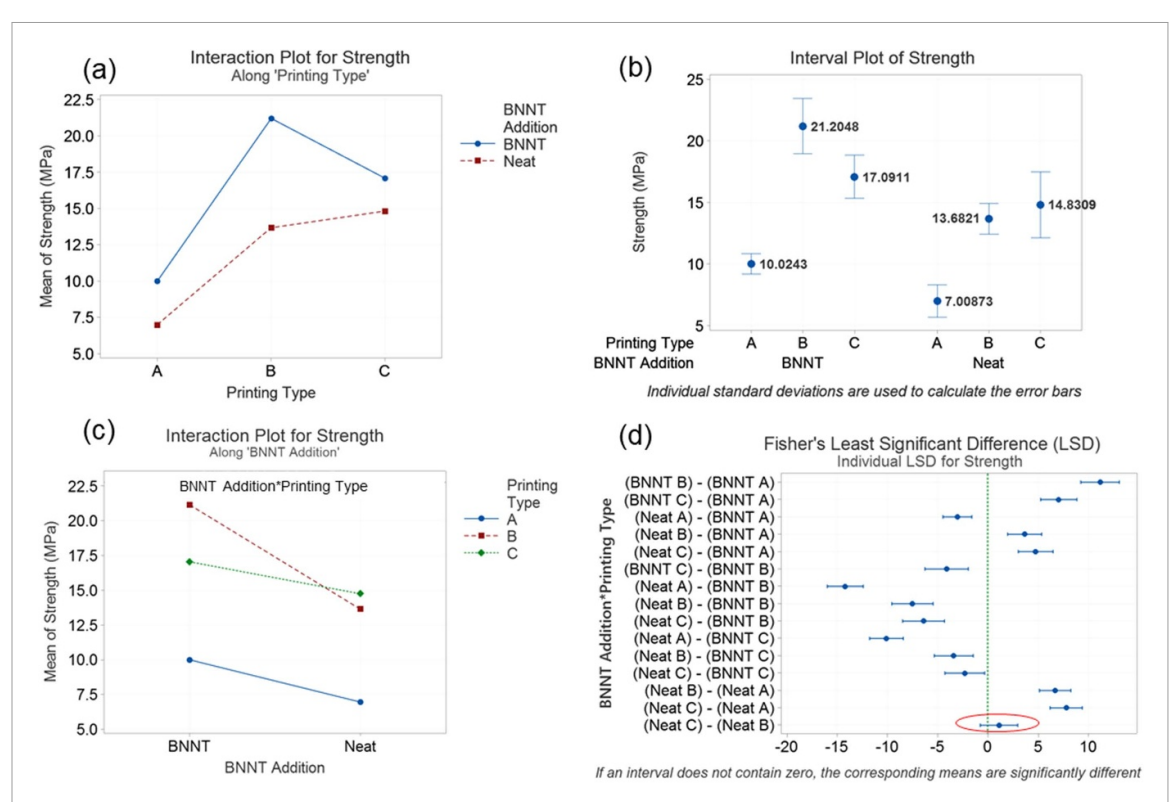


**Figure 8.** Plots for strength (a) Interaction plot along levels of factor 'printing types' (b) interval plot showing individual mean values of strength with error bars representing its standard deviation (c) interaction plot along levels of factor 'BNNT addition' (d) individual Fisher's least significant difference (LSD) representing insignificant combination through the red circle.

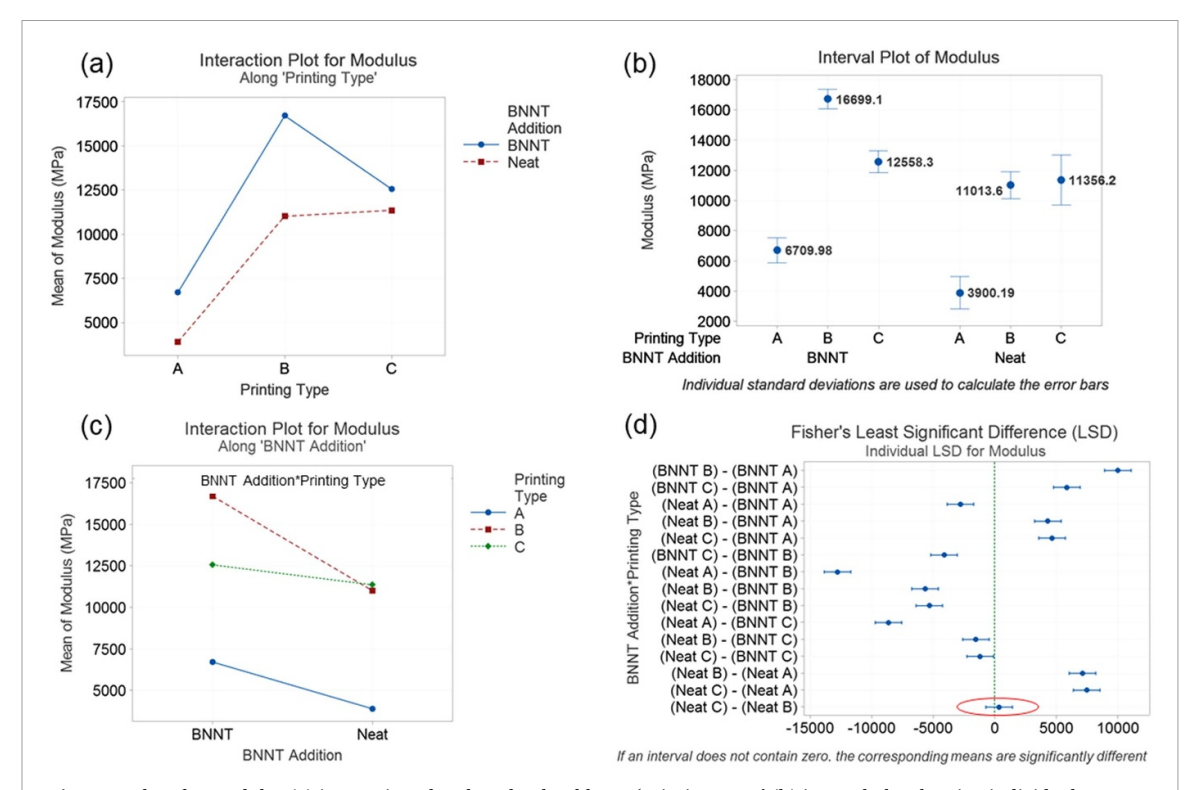


**Figure 9.** Plots for modulus (a) interaction plot along levels of factor 'printing types' (b) interval plot showing individual mean values of modulus with error bars representing its standard deviation (c) interaction plot along levels of factor 'BNNT addition' (d) individual Fisher's least significant difference (LSD) representing insignificant combination through the red circle.

matrix proving the effective dispersion through the solvent mixing approach used in this study. Along with well-dispersed sites, the small bundles of BNNTs were also observed (shown through marked circles in figure 11). Significant improvements in mechanical strength and modulus of silica composites can be

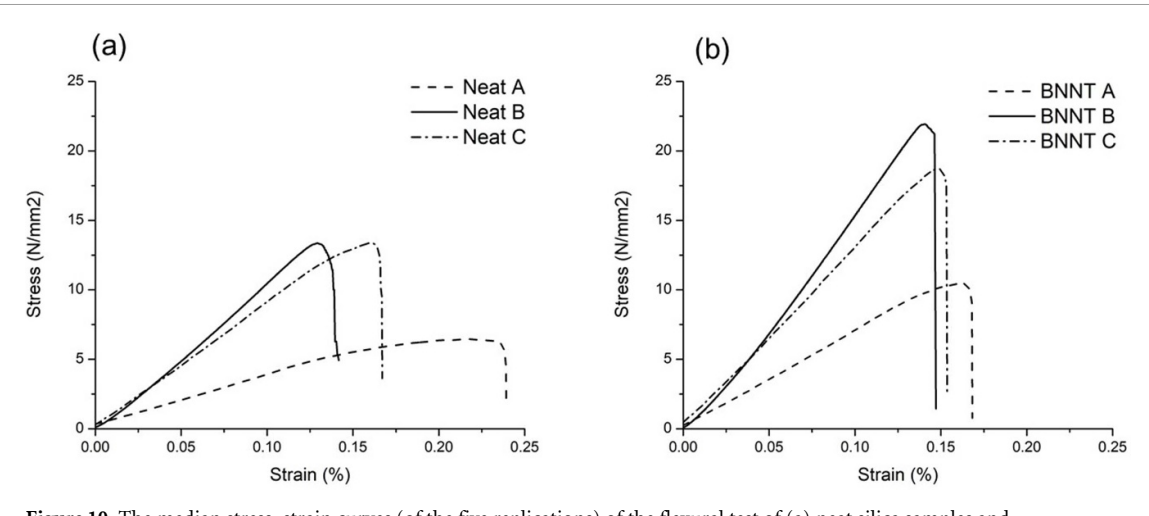
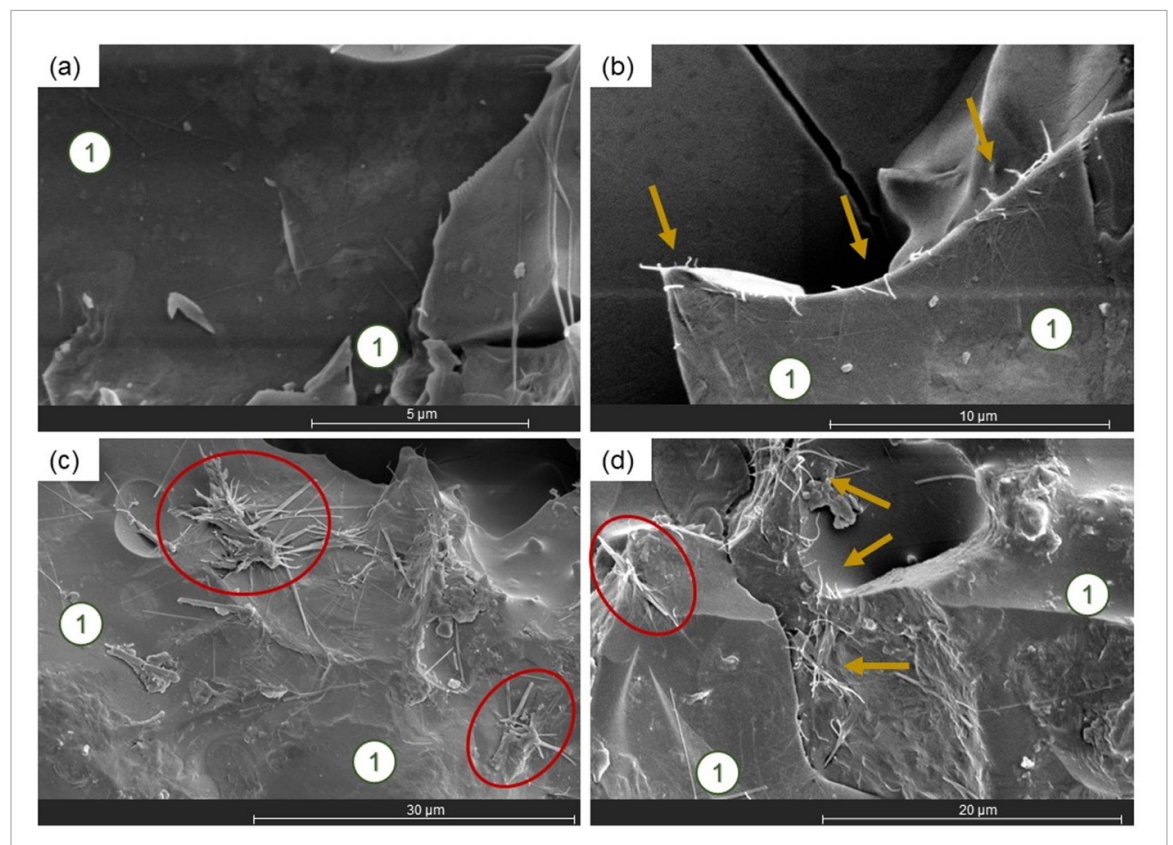


**Figure 10.** The median stress–strain curves (of the five replications) of the flexural test of (a) neat silica samples and (b) BNNT/silica composites samples.



**Figures 11.** (a)–(d) SEM images of the fracture surface of BNNT/silica samples. Marker '1' shows the region with individual nanotubes nicely embedded in the silica matrix. Yellow arrows in (b) and (d) show the pulled-out cantilever nanotubes during fracture. Red circles in (c) and (d) show the bundles of BNNTs embedded in the silica matrix.

attributed to added well-dispersed high aspect ratio nanotubes. During fracture, the nanotubes contribute as a reinforcement facing interfacial sliding failure (pull-out effect), which requires higher energy to propagate crack and strengthen the composite. Even at significantly less filler content, the pull-out effect of BNNTs with nanotubes coming out of the fracture plane was successfully captured under SEM (shown through arrows in figures 11(b) and (d), and figures 12(a)-(f)). These pulled-out cantilever nanotubes with one end embedded and the other end coming out from the fractured surface of the matrix confirms that the reinforcement through nanotubes effectively contributed toward mechanical load transfer during fracture, which strengthens the composite.

While working with nanotube composites, the dispersion of nanotubes is always a concern. Highly entangled structures must be effectively broken while mixed into a matrix to avoid microvoids around the

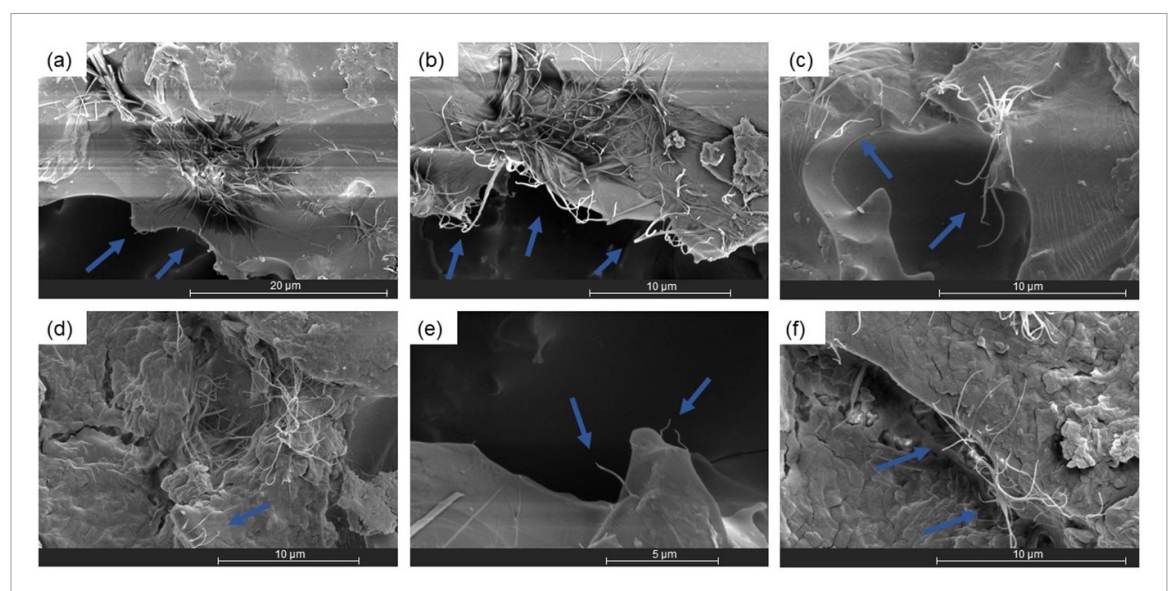


**Figure 12.** SEM images of the fractured surface with nicely embedded clusters having no voids around the nanotubes of a cluster. Blue arrows show the pulled-out cantilever nanotubes during fracture.

nanotubes of a cluster. It is well known that the cluster of nanotubes in a matrix acts as a stress concentrator and may reduce the mechanical performance if it contains microvoids around them, as matrix material face difficulty getting infused and filling the space around the nanotubes in a cluster. However, instead of acting as a stress concentrator, the clusters wholly embedded in the matrix show a positive bridging effect in the nearby areas.

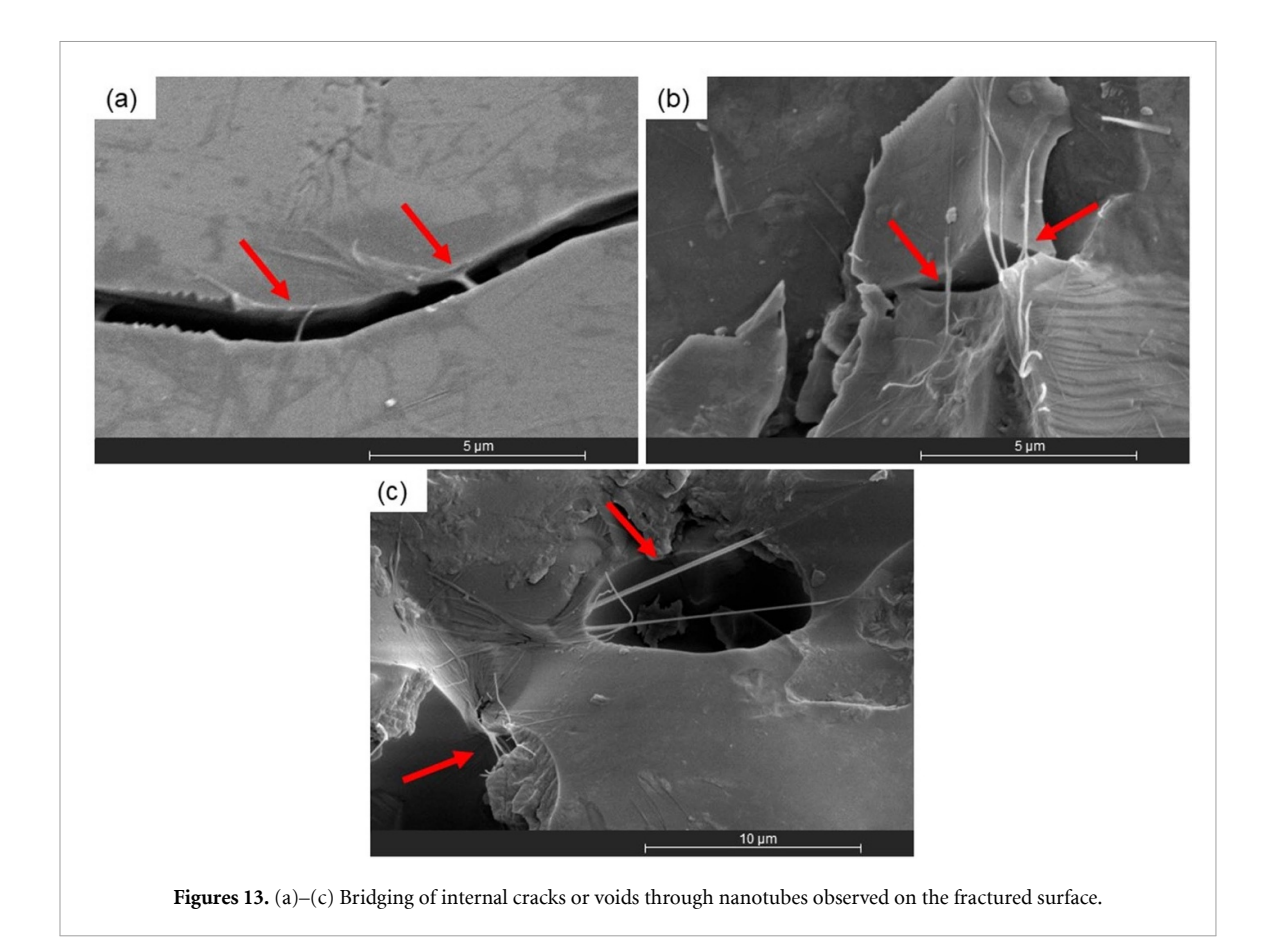
Along with well-dispersed sites, completely embedded BNNT clusters were also observed during SEM analysis of the fractured surface of the BNNT/silica composite (figure 12). These clusters of nanotubes having no voids/pockets around them (figures 12(a), (b), and (d)) gives strong evidence of having efficient load transfer between matrix and nanofiller, which can also be seen through consistent improvements in strength and modulus across all three types of samples. No clusters that lacked matrix material created microvoids were found during SEM analysis.

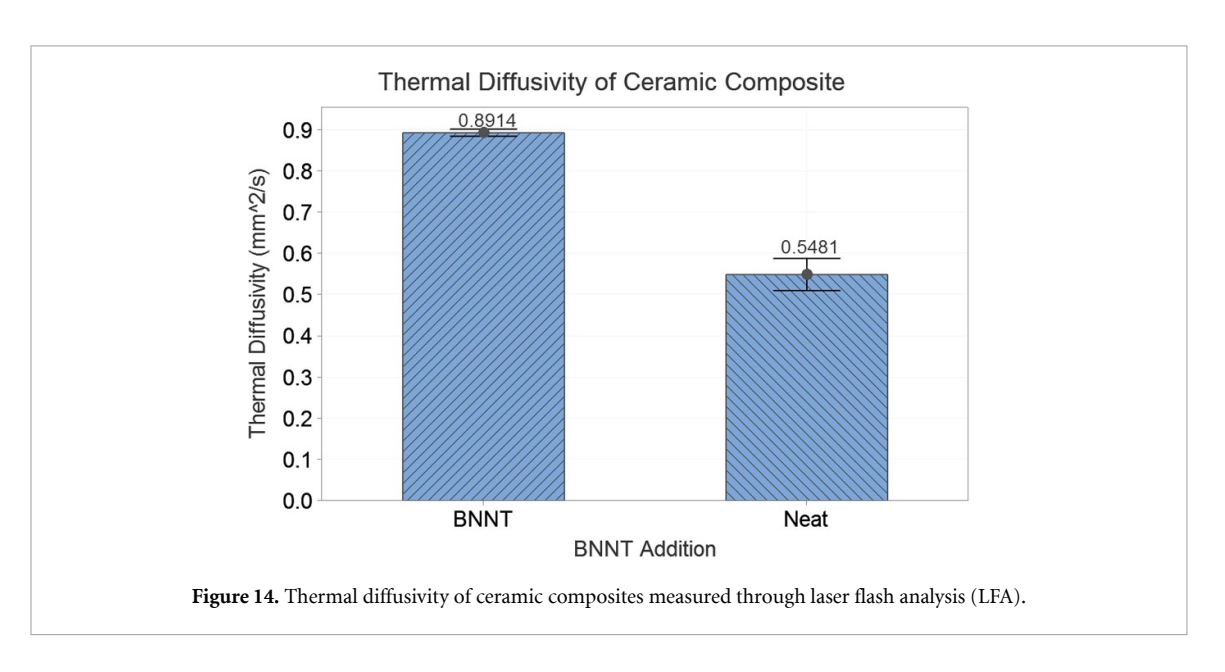
Not only the pull-out effect of nano reinforcements during fracture, but nanotubes also contributed to the bridging of internal cracks and voids formed during the fusing of silica powder. Arrows in the SEM images, figures 13(a)–(c), show the internal bridging behavior of nanotubes captured on the fractured surface. Since the fused ceramics are expected to be porous, containing voids ranging from nano to micro scale, the possibility of nanotubes contributing towards bridging internal cracks or voids could be a prominent strengthening phenomenon. Silica powder containing BNNTs, after polymer burnout, embeds nanotubes within themselves when exposed to high temperatures for fusing. Due to the longer length of BNNTs, up to several hundred micrometers, both ends of a nanotube can be embedded in silica particles far from each other, having a void/crack in between, creating an internal bridging effect. A significant mechanical strengthening observed in the printed fused BNNT/silica samples across all three printing types through internal crack/void bridging behavior and effective reinforcement during fracture (pull-out effect) explains that the higher aspect ratio BNNTs are the perfect candidate for 3D printed-fused ceramics.

#### 3.3. Thermal diffusivity testing

Laser flash analysis (LFA) was performed to measure the thermal diffusivity of the 3D-printed ceramic composites. The effect of nanofiller geometry was also observed in thermal diffusivity results, as shown in figure 14. The BNNT/silica samples showed significant improvements in thermal diffusivity by 62.63% at 25 °C testing temperature. Such significant enhancement and consistent results at very low filler content can be attributed to the excellent dispersion of BNNTs. The reported thermal diffusivity of the neat fused silica in previous literature is observed in the range of 0.50–0.65 mm $^2$  s $^{-1}$  [40, 41] at the reported density and 740 J kg $^{-1}$  K $^{-1}$  specific heat [42] which completely aligns with the results of this study.

The graphic in figure 15 shows a representative volume element (RVE) with 0.16 vol% of BNNT content (0.1 wt% of BNNTs in silica) with a high aspect ratio nanotube having a diameter ranging from 5 to 7 nm. The excellent dispersion along with clusters and bundles of BNNTs observed in SEM of BNNT/silica samples





can explain the improvements observed in its thermal diffusivity. Better dispersion allows BNNTs to extend themselves and effectively utilize their geometric benefit of tubular structures toward creating a thermally conductive network within the composite, as seen in figure 15(a). At the same time, figure 15(b) shows that bad dispersion creates clusters with percolation within the cluster but has less coverage of such good thermal transfer throughout the composite.

Neat silica samples, not containing any thermally conductive nanofillers, are observed to have more thermal diffusivity variability than BNNT/silica samples (figure 14). This variability in the measured thermal diffusivity of neat samples may be due to trapped voids, which, in BNNT composites, are filled/reinforced through thermally conductive nanotubes.

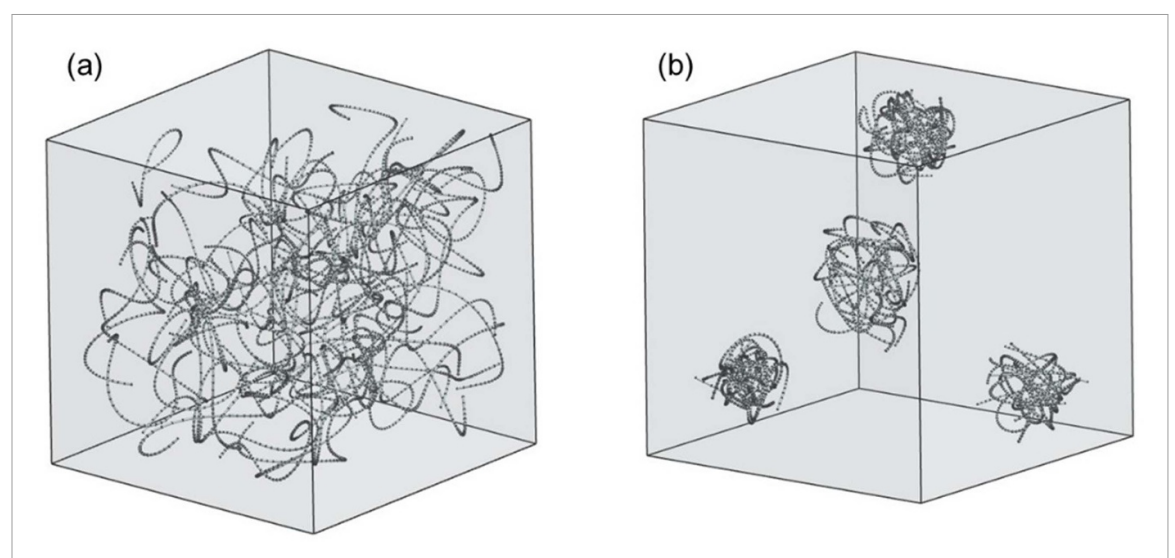


**Figure 15.** The representative volume element (RVE) of 0.16 vol% BNNT composite (a) with good dispersion of BNNTs allowing nanotubes to extend and create a thermally conductive network and (b) with dense cluster having a high gap between thermally conductive nanotube regions.

Stacked planner hexagonal-BN layers show good thermal transfer in the plane but poor thermal transfer along the direction perpendicular to the plane (between stacked planes). However, a tubular BN structure, having hexagonal-BN concentric planes in tubular form, makes it possible to solely utilize the high thermal conductivity of the planes while minimizing the effect of other crystal faces. Therefore, the long tubular structure is the effective nano reinforcement that creates a network and increases the thermal diffusivity when effectively dispersed with matrices. Combined DMA and LFA explain that the excellent dispersion of BNNTs, along with surviving longer aspect ratio tubes, is necessary for simultaneous enhancements in the composite's mechanical and thermal transfer properties successfully achieved through the solvent mixing method in this study.

#### 3.4. Finite Element Analysis

The development of a complete understanding of the structure-property relationship and the mechanism of interaction between nanofillers and matrix on the effective features of the resulting composite materials is aided by computer simulations and modeling of nanocomposites. A digital-twin simulation model was created to predict system behavior based on knowledge of process-structure-property correlation that occurs at a small scale. The factors affecting the simulation of nanotube reinforced composite like orientation, diameter, and waviness of nanotubes are kept most realistic for efficient predictions through simulation [43]. The RVE, as shown in figure 16(a), is prepared in Simcenter 3D software with randomized 3D orientation and waviness of nanotube having a controlled volume fraction of 0.16%. The volume fraction of nanotubes at 0.1 wt% content was calculated using the average density of fused neat ceramic across all three print directions (2.202 g cm<sup>-3</sup>) and the density of added nanofillers (1.38 g cm<sup>-3</sup> [44]).

The material properties of BNNTs (strength of 33 GPa [12], modulus of 1.3 TPa [13, 14], and Poisson's ratio of 0.05 [45]) and the average properties of ceramic matrix observed in this study across all three print directions (strength of 11.84 MPa, modulus of 8.76 GPa) were assigned to the RVE with the interfacial strength of BNNT/matrix of 34.70 MPa [32, 33]. The simulation was performed in Simcenter Multimech with the boundary conditions shown in figure 16(b). The crack propagation observed on a plane inside the RVE, as shown in figures 16(c) and (d), makes it evident that the crack initiated from the side of the matrix does not continue past the nanotube as it requires higher energy to propagate without deflection. A video showing crack propagation and stress in a nanotube is added in supporting information for a detailed understanding. Furthermore, low-level stress around the matrix and the high-level stress in the nanotube with only two ends embedded in the matrix indicates the effective load transfer between the matrix and filler, which improves the mechanical properties of the ceramics. Such modeling and simulation approaches explaining the detailed fracture mechanics can boost the development of future high-performance multifunctional nanocomposites.

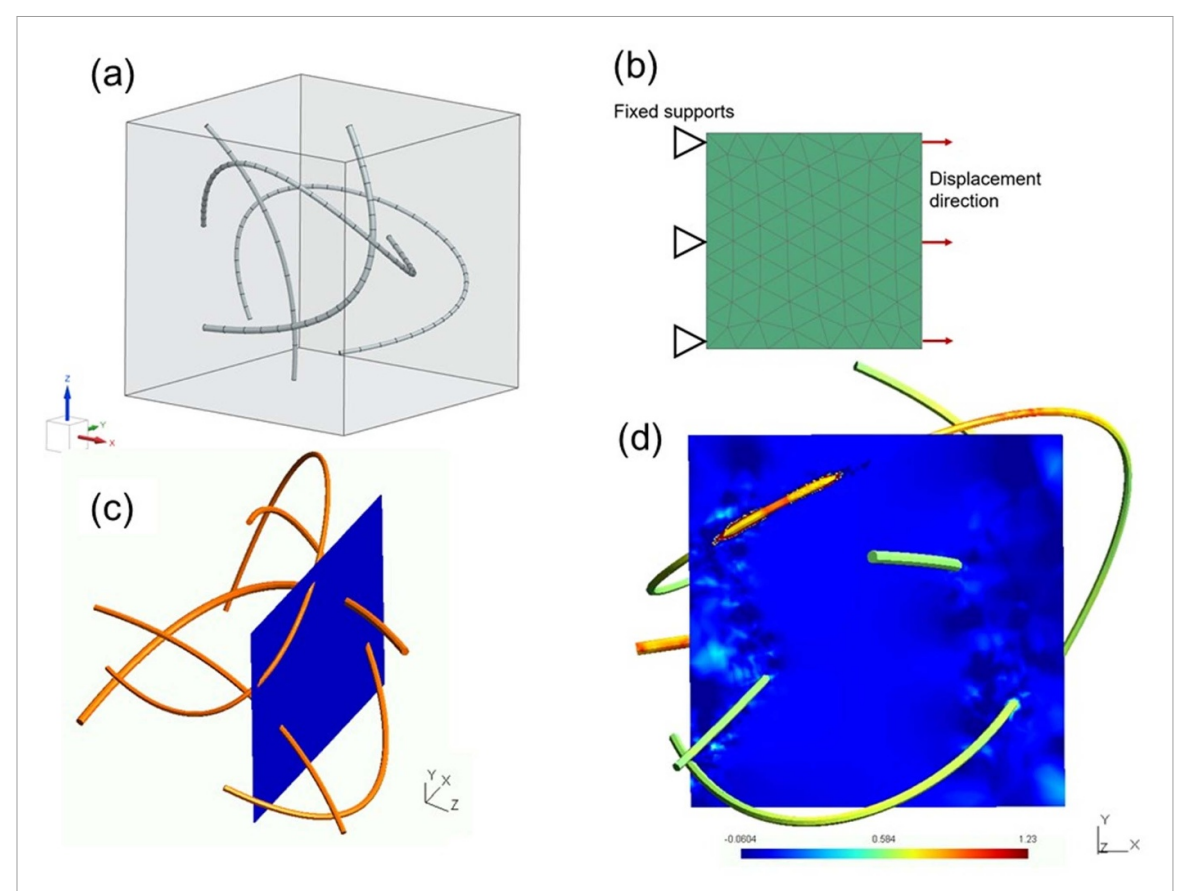


**Figure 16.** (a) Representative volume element (RVE) having 0.16 vol% BNNTs (b) boundary conditions and applied displacement during simulation (c) and (d) before and after displacement showing a plane of Stress11 levels in the RVE where crack propagation and effective reinforcement through BNNTs are studied.

#### 4. Conclusions

Multifunctional BNNTs, having a unique combination of properties such as high thermal stability, oxidation resistance, good mechanical properties, high thermal conductivity, electrically insulating, and radiation shielding, were effectively dispersed in a polymer suspension silica ceramic resin. In this paper, SLA 3D printed ceramic matrix composite having 0.1 wt% BNNTs were successfully fabricated, and their mechanical performance along all three print directions is characterized. The mechanical properties of printed ceramic composites examined using DMA showed statistically significant improvements up to 54.98% in bending strength and 72.04% in bending modulus with just 0.1 wt% of BNNT addition. The length scale effect of BNNTs having a longer aspect ratio at the nanoscale, bridging and pull-out effect of nanotubes, was successfully captured under SEM. Reinforcement through effective load transfer and crack propagation mechanism was also studied through finite element analysis of BNNT ceramic matrix composite. Furthermore, significant improvements of 62.63% were observed in the ceramic's thermal diffusivity measured using LFA. This unique combination of improved mechanical performance, thermal conduction with preserved electrical insulation properties, chemical inertness, high-temperature survivability, and radiation shielding properties could open a wide range of deep space applications.

## Acknowledgment

The authors would like to thank the National High-Magnetic Field Laboratory for SEM support.

## **Funding**

This research was funded by Florida State University start-up funds. The authors would like to thank the Industrial and Manufacturing Engineering (IME) Summer Research Experience for Undergraduates (REU)

from NSF and DREAM/RETREAT/RISE/CREST programs at the FAMU-FSU College of Engineering for their funding and support.

#### **Author contributions**

The manuscript was written through contributions of all authors. All authors have given approval to the final version of the manuscript.

#### **ORCID iD**

Mehul Tank https://orcid.org/0000-0002-6011-0354

#### References

- [1] Moon S K, Tan Y E, Hwang J and Yoon Y-J 2014 Application of 3D printing technology for designing light-weight unmanned aerial vehicle wing structures *Int. J. Precis. Eng. Manuf.*—*Green Technol.* 1 223–8
- [2] Melchels F P W, Feijen J and Grijpma D W 2010 A review on stereolithography and its applications in biomedical engineering Biomaterials 31 6121–30
- [3] Chia H N and Wu B M 2015 Recent advances in 3D printing of biomaterials J. Biol. Eng. 9 4
- [4] Leigh S J, Bradley R J, Purssell C P, Billson D R and Hutchins D A 2012 A simple, low-cost conductive composite material for 3D printing of electronic sensors *PLoS One* 7 e49365
- [5] Zocca A, Colombo P, Gomes C M and Günster J 2015 Additive manufacturing of ceramics: issues, potentialities, and opportunities J. Am. Ceram. Soc. 98 1983–2001
- [6] Deckers J 2014 Additive manufacturing of ceramics: a review J. Ceram. Sci. Technol. 5 245-260
- [7] Halloran J W 2016 Ceramic stereolithography: additive manufacturing for ceramics by photopolymerization Annu. Rev. Mater. Res. 46 19–40
- [8] Tank M and Sweat R 2022 Boron nitride nanotubes (BNNTs) and BNNT composites: a review *Mater. Perform. Charact.* 11 20220042
- [9] Blase X, Rubio A, Louie S G and Cohen M L 1994 Stability and band gap constancy of boron nitride nanotubes Europhys. Lett. 28 335–40
- [10] Rubio A, Corkill J L and Cohen M L 1994 Theory of graphitic boron nitride nanotubes Phys. Rev. B 49 5081-4
- [11] Chopra N G, Luyken R J, Cherrey K, Crespi V H, Cohen M L, Louie S G and Zettl A 1995 Boron nitride nanotubes *Science* **269** 966–7
- [12] Wei X, Wang M-S, Bando Y and Golberg D 2010 Tensile tests on individual multi-walled boron nitride nanotubes *Adv. Mater.*
- [13] Chopra N G and Zettl A 1998 Measurement of the elastic modulus of a multi-wall boron nitride nanotube Solid State Commun. 105 297–300
- [14] Arenal R, Wang M-S, Xu Z, Loiseau A and Golberg D 2011 Young modulus, mechanical and electrical properties of isolated individual and bundled single-walled boron nitride nanotubes *Nanotechnology* 22 265704
- [15] Tanur A E, Wang J, Reddy A L M, Lamont D N, Yap Y K and Walker G C 2013 Diameter-dependent bending modulus of individual multiwall boron nitride nanotubes *J. Phys. Chem.* B 117 4618–25
- [16] Chen Y, Zou J, Campbell S J and Le Caer G 2004 Boron nitride nanotubes: pronounced resistance to oxidation Appl. Phys. Lett. 84 2430–2
- [17] Chen X, Dmuchowski C M, Park C, Fay C C and Ke C 2017 Quantitative characterization of structural and mechanical properties of boron nitride nanotubes in high temperature environments *Sci. Rep.* 7 11388
- [18] Ghassemi H M, Lee C H, Yap Y K and Yassar R S 2010 *In situ* TEM monitoring of thermal decomposition in individual boron nitride nanotubes *JOM* 62 69–73
- [19] Tank M J, Reyes A N, Park J G, Scammell L R, Smith M W, de Leon A and Sweat R D 2022 Extreme thermal stability and dissociation mechanisms of purified boron nitride nanotubes: implications for high-temperature nanocomposites ACS Appl. Nano Mater. 5 12444–53
- [20] Chang C W, Fennimore A M, Afanasiev A, Okawa D, Ikuno T, Garcia H, Li D, Majumdar A and Zettl A 2006 Isotope effect on the thermal conductivity of boron nitride nanotubes *Phys. Rev. Lett.* **97** 085901
- [21] Cumings J and Zettl A 2004 Field emission and current-voltage properties of boron nitride nanotubes Solid State Commun. 129 661–4
- [22] Lee C H, Xie M, Kayastha V, Wang J and Yap Y K 2010 Patterned growth of boron nitride nanotubes by catalytic chemical vapor deposition *Chem. Mater.* 22 1782–7
- [23] Wilder J W G, Venema L C, Rinzler A G, Smalley R E and Dekker C 1998 Electronic structure of atomically resolved carbon nanotubes Nature 391 59–62
- [24] Cheraghi E, Chen S and Yeow J T W 2021 Boron nitride-based nanomaterials for radiation shielding: a review *IEEE Nanotechnol.* Mag. 15 8–17
- [25] Ghazizadeh M, Estevez J E and Kelkar A D Joint school of nanoscience and nanoengineering, north carolina A&T state university and university of north carolina at greensboro, USA 2015 boron nitride nanotubes for space radiation shielding *Int. J. Nano Stud. Technol.* 4 1–2
- [26] Estevez J E, Ghazizadeh M, Ryan J G and Kelkar A D 2014 Simulation of hydrogenated boron nitride nanotube's mechanical properties for radiation shielding applications Int. J. Chem. Mat. Biomol. Sci 8 5
- [27] Choi S R, Bansal N P and Garg A 2007 Mechanical and microstructural characterization of boron nitride nanotubes-reinforced SOFC seal glass composite Mater. Sci. Eng. A 460–1 509–15
- [28] Xu J-J, Bai Y-J, Wang W-L, Wang S-R, Han F-D, Qi Y-X and Bi J-Q 2012 Toughening and reinforcing zirconia ceramics by introducing boron nitride nanotubes *Mater. Sci. Eng.* A 546 301–6

- [29] Wang W-L, Bi J-Q, Wang S-R, Sun K-N, Du M, Long N-N and Bai Y-J 2011 Microstructure and mechanical properties of alumina ceramics reinforced by boron nitride nanotubes *J. Eur. Ceram. Soc.* 31 2277–84
- [30] Du M, Bi J-Q, Wang W-L, Sun X-L and Long N-N 2011 Microstructure and properties of SiO<sub>2</sub> matrix reinforced by BN nanotubes and nanoparticles J. Alloys Compd. 509 9996–10002
- [31] Lu X, Dolmetsch T, Zhang C, Chen Y, Boesl B and Agarwal A 2021 *In-situ* synthesis of boron nitride nanotube reinforced aluminum oxide composites by molecular mixing *Ceram. Int.* 47 13970–9
- [32] Li N, Dmuchowski C M, Jiang Y, Yi C, Gou F, Deng J, Ke C and Chew H B 2022 Sliding energy landscape governs interfacial failure of nanotube-reinforced ceramic nanocomposites Scr. Mater. 210 114413
- [33] Yi C, Bagchi S, Gou F, Dmuchowski C M, Park C, Fay C C, Chew H B and Ke C 2019 Direct nanomechanical measurements of boron nitride nanotube—ceramic interfaces *Nanotechnology* 30 025706
- [34] Jia Y, Ajayi T D, Morales J, Chowdhury M A R, Sauti G, Chu S, Park C and Xu C 2019 Thermal properties of polymer-derived ceramic reinforced with boron nitride nanotubes *J. Am. Ceram. Soc.* 102 7584–93
- [35] Tiano A L, Gibbons L, Tsui M, Applin S I, Silva R, Park C and Fay C C 2016 Thermodynamic approach to boron nitride nanotube solubility and dispersion Nanoscale 8 4348–59
- [36] Li H, Hu K, Liu Y, Lu Z and Liang J 2021 Improved mechanical properties of silica ceramic cores prepared by 3D printing and sintering processes Scr. Mater. 194 113665
- [37] Bae C-J, Kim D and Halloran J W 2019 Mechanical and kinetic studies on the refractory fused silica of integrally cored ceramic mold fabricated by additive manufacturing J. Eur. Ceram. Soc. 39 618–23
- [38] Wang Y, Wang Z, Liu S, Qu Z, Han Z, Liu F and Li L 2019 Additive manufacturing of silica ceramics from aqueous acrylamide based suspension *Ceram. Int.* 45 21328–32
- [39] Dong W, Ma H, Liu R, Liu T, Li S, Bao C and Song S 2021 Fabrication by stereolithography of fiber-reinforced fused silica composites with reduced crack and improved mechanical properties Ceram. Int. 47 24121–9
- [40] Li X, Yan L, Zhang Y, Yang X, Guo A, Du H, Hou F and Liu J 2022 Lightweight porous silica ceramics with ultra-low thermal conductivity and enhanced compressive strength Ceram. Int. 48 9788–96
- [41] Wray K L and Connolly T J 1959 Thermal conductivity of clear fused silica at high temperatures J. Appl. Phys. 30 1702-5
- [42] Fused silica specific heat (available at: http://accuratus.com/fused.html)
- [43] Patadia M H, Tank M J, de Leon A and Sweat R D 2023 Digital twins of high aspect ratio wavy nanotube composite performance for model-informed manufacturing Scr. Mater. 226 115192
- [44] Zhi C, Bando Y, Tang C and Golberg D 2011 Specific heat capacity and density of multi-walled boron nitride nanotubes by chemical vapor deposition Solid State Commun. 151 183–6
- [45] Sakharova N A, Antunes J M, Pereira A F G, Chaparro B M and Fernandes J V 2021 On the determination of elastic properties of single-walled boron nitride nanotubes by numerical simulation *Materials* 14 3183